JOURNAL OF APPLIED PHYSICS **118**, 225101 (2015)

Ab initio study of anisotropic mechanical properties of $LiCoO_2$ during lithium intercalation and deintercalation process

Linmin Wu and Jing Zhang[a)]
Department of Mechanical Engineering, Indiana University-Purdue University Indianapolis, Indianapolis, Indiana 46202, USA

(Received 7 July 2015; accepted 25 November 2015; published online 14 December 2015)

The mechanical properties of Li_xCoO_2 under various Li concentrations and associated anisotropy have been systematically studied using the first principles method. During the lithium intercalation process, the Young's modulus, bulk modulus, shear modulus, and ultimate strength increase with increasing lithium concentration. Strong anisotropy of mechanical properties between a-axis and c-axis in Li_xCoO_2 is identified at low lithium concentrations, and the anisotropy decreases with increasing lithium concentration. The observed lithium concentration dependence and anisotropy are explained by analyzing the charge transfer using Bader charge analysis, bond order analysis, and bond strength by investigating partial density of states and charge density difference. With the decrease of Li concentration, the charge depletion in the bonding regions increases, indicating a weaker Co-O bond strength. Additionally, the Young's modulus, bulk modulus, shear modulus, and toughness are obtained by simulating *ab initio* tensile tests. From the simulated stress-strain curves, Li_xCoO_2 shows the highest toughness, which is in contraction with Pugh criterion prediction based on elastic properties only. © *2015 AIP Publishing LLC*.
[http://dx.doi.org/10.1063/1.4937409]

I. INTRODUCTION

Efficient and durable energy storage is one of the major factors limiting the development of renewable energy. Since lithium-ion batteries were first commercialized by Sony in 1991, they have played a significant role in energy storage devices. One of the popular cathode materials in lithium-ion (Li-ion) batteries is lithium cobalt oxide ($LiCoO_2$) developed by Goodenough and Mizushima in 1980s.[1] Due to its excellent electrochemical properties of $LiCoO_2$, it becomes one of the most widely used cathode materials in lithium-ion batteries.[2]

A critical challenge in advanced lithium-ion batteries is preventing fracture and mechanical failure of electrodes during lithium intercalation and deintercalation processes. Large volume expansion, phase transition, and associated Li diffusion-induced stresses within electrode materials can lead to their fracture and failure, which result in battery capacity loss and power fade. For $LiCoO_2$, it is found that capacity faded about 2.2% and 6.5% for exchange of 0.5 Li per CoO_2 after 10 and 50 charge-discharge cycles and accompanied with a decrease of Co-O bond length using X-ray absorption spectroscopy.[3] A transmission electron microscopy (TEM) study showed that 20% of the $LiCoO_2$ particles were indeed fractured after 50 cycles at a 0.2 C rate between 2.5 V and 4.35 V.[4] Thus it is important to understand the mechanical properties of $LiCoO_2$ during lithium intercalation and deintercalation processes.

There are several works on investigating the mechanical properties of pure $LiCoO_2$. Hart and Bates[5] calculated the elastic constants of $LiCoO_2$ using atomistic empirical potential model. Their results estimated the Young's modulus in the range of 315–516 GPa. Wang *et al.*[4] reported the bulk modulus of $LiCoO_2$ 149 ± 2 GPa using high-pressure synchrotron X-ray powder diffraction (XRD) experiments. They also did density functional theory (DFT) calculations of bulk modulus of 168.5 and 142.9 GPa using the local density approximation (LDA) and generalized gradient approximation (GGA), respectively. Recently, Qi *et al.*[6] demonstrated the averaged Young's modulus of $LiCoO_2$ with 264 GPa, and CoO_2 with 98.5 GPa using a hybrid functional (HSE06).

In terms of anisotropy, Diercks *et al.*[7] experimentally studied the anisotropic mechanical behavior in cycled $LiCoO_2$. Nanoindentation was performed on individual $LiCoO_2$ particles. Fractures in these particles exhibited anisotropic behavior, which was confirmed by electron microscopy and diffraction examination indicating both intra- and inter-granular fracture occurred on (001) planes.

Isotropic mechanical properties have been used in almost all of the Li-ion battery models in literature without taking into account of Li content effect on mechanical properties. The reason is that these mechanical properties, such as Young's modulus, elastic constants, bulk modulus, and shear modulus, are not completely available in literature, likely due to experimental challenges. Hence theoretical study of anisotropic and Li content dependent mechanical properties of single crystal Li_xCoO_2 is warranted.

In this paper, anisotropic and Li concentration dependent mechanical properties will be studied systematically. To our best knowledge, these properties have not been reported in the literature. The paper will be organized as follows: In Section II, the details of DFT calculation are given to describe the strategy of modeling Li_xCoO_2 under various Li

[a)]Author to whom correspondence should be addressed. Electronic mail: jz29@iupui.edu. Tel.: 317-278-7186. Fax: 317-274-9744.

concentrations. In Section III, the elastic properties of Li_xCoO_2 under various Li concentrations are calculated using both energy strain approach and stress strain approach. Bond order analysis, partial density of states (PDOS), charge density difference, and Bader charge analysis are employed to investigate the anisotropic and Li concentration dependent mechanical properties. A relationship to estimate the Young's modulus and ultimate strength of Li_xCoO_2 at various lithium concentrations is proposed. Conclusion is given in Section IV.

II. COMPUTATIONAL DETAILS

The mechanical properties of Li_xCoO_2 are calculated using the DFT method.[8,9] The exchange correlation energy and potential are described as GGA in the scheme of Perdew–Burke–Ernzerhof (PBE).[10,11] The projected augmented wave (PAW) method[12,13] is used, as implemented in the Vienna *ab intio* Simulation Package (VASP)[14,15] and Cambridge Serial Total Energy Package (CASTEP).[16] GGA functionals are selected because they are more reliable than LDA functionals for predicting transition metal systems.[17] Because *d* orbital plays an important role in coordinating for transition metals, the U (on-site coulomb term) value for Co-3*d* is selected to be 4.91 eV according to the literature.[18]

Li_xCoO_2 calculations are performed with a $2 \times 2 \times 1$ supercell (Fig. 1). For $x = 0.5$, 0.75, and 1, the Li_xCoO_2 configurations are chosen same as described in Ref. 19. The convergence tests of the total energy with respect to the *k*-points sampling and cut-off energy have been carefully examined; these ensure that the total energy is converged to within 10^{-5} eV per formula unit. The Monkhorst–Pack[20] scheme $3 \times 3 \times 1$ *k*-points mesh is used for the integration in the irreducible Brillouin zone. Energy cut-off for the plane waves is chosen to be 500 eV. Before the calculation, both the lattice parameters and the ionic positions are fully relaxed, and the final forces on all relaxed atoms are less than 0.005 eV/Å.

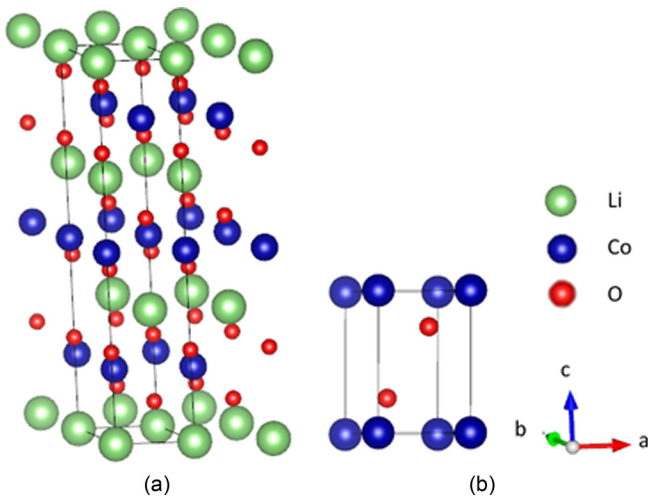

FIG. 1. (a) The $2 \times 2 \times 1$ super cell of $LiCoO_2$. The unit cell is the cell in solid line, (b) unit cell of CoO_2. The green balls are Li atoms. The red balls are oxygen atoms. The blue balls are cobalt atoms.

In principle, there are two ways of computing single crystal mechanical properties from *ab initio* methods: the energy-strain approach and the stress-strain approach. The energy-strain approach is based on the computed total energies of properly selected strained states of the crystal. The stress-strain approach, on the other hand, relies on the feature of VASP to directly calculate the stress tensor. Both methods will be used in this study.

For the energy-strain approach, elastic constants can be obtained by analyzing energies under different small strain patterns in VASP and CASTEP. A finite strain amplitude is specified for each strain pattern. Once elastic constants are determined, Young's modulus and Poisson's ratio can be deduced. It is noted that the calculations have an assumption of small elastic strain deformations.

To investigate the mechanical properties in large deformations until fracture, simulated tensile tests (stress-strain approach) are performed using the first principles method implemented in VASP. Strain increments are continuously applied to the cell along tensile directions. For each strain, ions are allowed to be relaxed so that the stress in other directions is minimized. Stress components can be directly obtained from the simulation result files. Once the stress-strain curve is obtained, the Young's modulus along the direction of strain can be computed from the first derivatives of the stresses, and toughness can be calculated from the integral of the area below the stress-strain curve.

III. RESULTS AND DISCUSSION

The calculated $LiCoO_2$ lattice parameters are $a = b = 2.84$ Å, $c = 14.16$ Å, $\alpha = \beta = 90°$, $\gamma = 120°$,[21] with literature experimental data[22,23] and computational results[6,24] included in Table I. The optimized volume of our calculation is generally in good agreement with the literature data and is slightly greater than the experimental data.[23] Further delithiated phase calculations of Li_xCoO_2 are based on the relaxed unit cell. For CoO_2, the relaxed CoO_2 has the following lattice parameters, $a = b = 2.86$ Å, $c = 4.79$ Å, $\alpha = \beta = 90°$, $\gamma = 120°$. The volume of CoO_2 is 33.93 $Å^3$, which is about 2.9% bigger than that of $LiCoO_2$. This indicates a volume change during Li intercalation and deintercalation cycling.

A. Li concentration dependent elastic properties

To calculate the Li concentration dependent elastic properties, the ground states with the lowest energy configuration of Li_xCoO_2 for $x = 0.5$, 0.75, and 1 are selected. The initial configurations are chosen as described in Ref. 19. CoO_2 is also used for comparison. The reason of selecting these three configurations Li_xCoO_2 ($x = 0.5$, 0.75, and 1) is

TABLE I. Lattice parameters and volume of $LiCoO_2$.

	a & b (Å)	c (Å)	V ($Å^3$)
This work	2.84	14.16	32.96
Experiment[22,23]	2.82	14.05	32.23
Xiong *et al.*[24] (GGA)	2.84	14.17	32.99
Qi *et al.*[6] (HSE06)	2.80	14.07	31.84

that there are phase transitions at low and medium Li concentrations ($x < 0.5$). Reimers and Dahn[25] observed that Li_xCoO_2 transformed to a monoclinic structure at 0.5 Li concentration using *in situ* X-ray diffraction measurement. Van der Ven *et al.*[26] established the phase diagram using the density functional theory calculations coupled with cluster expansion method. They confirmed the phase transitions occurred at low and medium lithium concentrations.

The calculated Li concentration dependent elastic properties using energy-strain approach are listed in Table II. For pure $LiCoO_2$, the Young's modulus has the same value along the X- and Y-axis directions due to the symmetry of the structure. In this work, the X-Y plane is located in the plane composed by *a* and *b* crystallographic axes. The Z axis is the *c* crystallographic axis. To calibrate the model, a comparison with the results using CASTEP and literature data is conducted. As shown in Table II, the results obtained from CASTEP are slightly lower than those from VASP. This may be caused by the different algorithms implemented in two software packages. For the Young's modulus, Hart and Bates[5] applied the energy-strain approach to calculate the elastic constants using GULP. The results were in the range of 315–516 GPa. The discrepancy may be caused by their atomistic empirical potentials. Qu *et al.*[27] studied the Young's moduli of polycrystalline $LiCoO_2$ grains were measured to be 151–236 GPa using nano-indentation experiment. Wang *et al.*[28] reported the Young's modulus of $LiCoO_2$ powder was about 171 GPa obtained from high-pressure synchrotron XRD experiments. Because the material used in this study is a single crystal, it is reasonable to get a higher Young's modulus than experiment. Wang *et al.*[4] reported bulk modulus 168 GPa using the DFT calculations, and the result is consistent with this study. With single crystal data, the elastic properties of the polycrystalline can be approximately estimated by using the Voigt–Reuss–Hill homogenization scheme,[29] and they are also included in Table II.

Lithium concentration has a profound effect on the elasstic properties of Li_xCoO_2. As shown in Table II, $LiCoO_2$ shows a very large increase of effective Young's modulus compared with that of CoO_2, which is about 200% higher. This is mainly due to the increase of Young's modulus in Z direction. Without the Li ions, the layers of CoO_2 are weakly bonded by van der Waals forces.[30] With the increase of the Li concentration ($0.5 < x < 1$), the Young's moduli in X-axis direction increase from 270.97 GPa to 321.05 GPa; meanwhile in Z-axis direction, the Young's moduli increase from 106.36 GPa to 212.83 GPa. The bulk modulus, shear modulus share the same trend as the Young's modulus.

TABLE II. Elastic properties of Li_xCoO_2 for $x = 0$, 0.5, 0.75 and 1. Bulk modulus (B), shear modulus (G) and Young's modulus (E) are included. Subscripts H, R and V represents the results using the Voigt-Reuss-Hill homogenization scheme.[40]

	VASP				CASTEP	
	CoO_2	$Li_{0.5}CoO_2$	$Li_{0.75}CoO_2$	$LiCoO_2$	CoO_2	$LiCoO_2$
E_X (GPa)	261.38	270.97	275.51	321.05	242.62	290.06
E_Z (GPa)	75.89	106.36	135.19	212.83	51.36	177.25
E_{VRH} (GPa)	108.52	145.83	165.74	252.09	99.83	234.51
B (GPa)	68.69	100.65	110.35	166.74	58.67	123.67
B_H (GPa)	96.87	113.74	119.25	171.95	71.87	129.26
B_R (GPa)	68.69	100.65	110.35	166.75	58.67	123.17
B_V (GPa)	125.05	127.34	128.15	177.16	95.07	135.34
G_H (GPa)	41.71	58.63	65.34	111.38	31.66	86.68
G_R (GPa)	18.95	43.72	55.30	96.01	9.85	82.25
G_V (GPa)	64.46	72.96	74.89	104.75	53.47	91.10

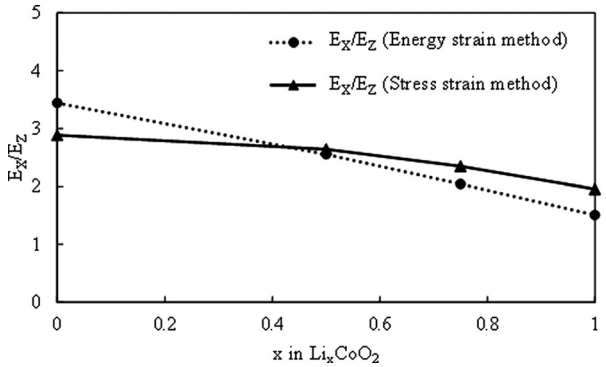

FIG. 2. Anisotropy of Young's modulus in Li_xCoO_2 as a function of Li concentration.

B. Anisotropy of Young's modulus

It is noted that in Table II, the Young's moduli show different values depending on axis directions. The ratio of E_X/E_Z is defined to describe the anisotropy of Li_xCoO_2. Using the data in Table II, the anisotroy of Young's modulus as a function of Li ion concentration is ploted in Fig. 2. Li_xCoO_2 shows a decreasing anisotropy with the increase of Li concentration. This is due to the fact that during deintercalation process or low Li concentration, Li ions leave the layered Li_xCoO_2 structure causing weak van der Waals bonds in Z-axis direction.[30] During intercalation process, on the other hand, Li ions fill the layered structure, producing a stronger bond in Z-axis direction, thus reducing anisotropy. To verify the preceding statement, bond order analysis[31–33] is employed to study the bonding between Li and CoO_2 layer. The results are listed in Table III. The bond order of Li-CoO_2 is 0, 0.37, 0.40, and 0.42 for CoO_2, $Li_{0.5}CoO_2$, $Li_{0.75}CoO_2$, and $LiCoO_2$, respectively. The increase of bond order indicates the increasing bond strength in Z-axis direction with the insertion of Li ions. Due to this anisotropy of Young's modulus, the induced mechanical stresses during intercalation and deintercalation processes will be oscillated.

C. Stress-strain relation and toughness

Beyond elastic regions, it is also important to investigate large deformations. Experimentally, it is a daunting task to perform a tensile test on a brittle oxide material. In this

TABLE III. Bond orders in Li-CoO_2 in Li_xCoO_2.

	Bond order
CoO_2	0
$Li_{0.5}CoO_2$	0.37
$Li_{0.75}CoO_2$	0.40
$LiCoO_2$	0.42

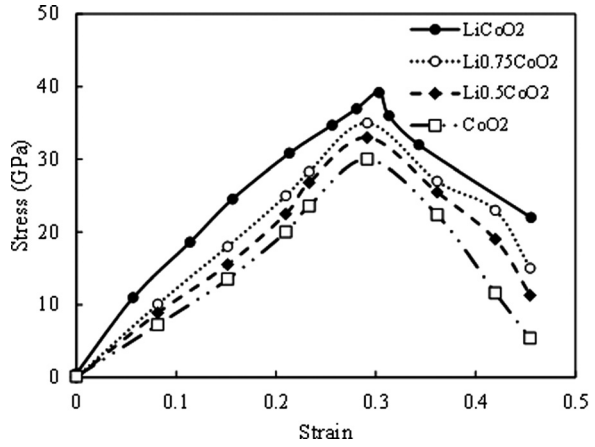

FIG. 3. Stress-strain curves of simulated tensile tests of CoO_2, $Li_{0.5}CoO_2$, $Li_{0.75}CoO_2$, and $LiCoO_2$ along Z direction.

study, the simulated stress-strain curves of Li_xCoO_2 are calcualted. From the stress-strain curve, three important mechanical properties can be evaluated: Young's modulus, ultimate strength, and toughness.

The stress-strain curves of CoO_2, $Li_{0.5}CoO_2$, $Li_{0.75}CoO_2$, and $LiCoO_2$ along Z- and X-axis directions are shown in Figs. 3 and 4, respectively. Because of the symmetry between X and Y axes, only the strain along the X axis is applied. The slope of initial linear portion of the stress-strain curve represents the Young's modulus, which is shown in Table IV. The calculated Young's moduli are consistent with the results in Table II, which confirms the correctness of the data. The Young's modulus anisotropy Ex/Ez using the data in Table IV is plotted in Fig. 2. Clearly, the two methods yield a very similar concentration dependent anisotropy. It is noted that using energy strain approach may meet the numerical difficulties when computing the second derivatives of the total energy with respect to the strain.[34] This can explain why these two methods show slightly different values. Besides, the ultimate strengths, UTS, along X- and Z-axis directions increase with the increase of Li concentration, as shown in Table IV.

To determine the brittleness or toughness of ceramic materials, Pugh criterion, B_H/G_H, has been widely used,[35] where B_H and G_H are the bulk and shear modulus listed in Table II, respectively. In Pugh criterion, if $B_H/G_H \gtrsim 1.75$, the material

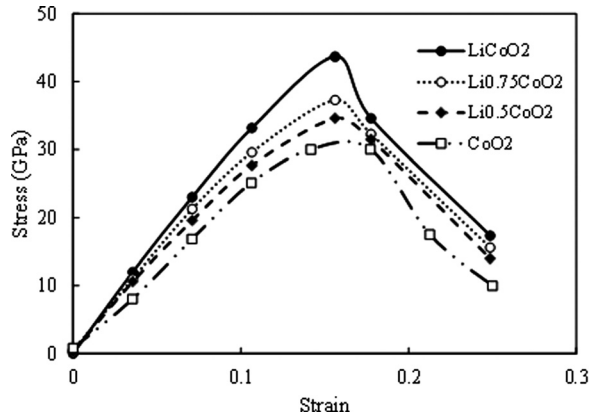

FIG. 4. Stress-strain curves of simulated tensile tests of of CoO_2, $Li_{0.5}CoO_2$, $Li_{0.75}CoO_2$, and $LiCoO_2$ along X direction.

TABLE IV. Mechanical properties obtained from *ab inito* tensile test. E is Young's modulus. UTS is ultimate strength. G_C is fracture toughness. The subscripts X and Z represent the directions.

	CoO_2	$Li_{0.5}CoO_2$	$Li_{0.75}CoO_2$	$LiCoO_2$
E_X (GPa)	250.36	276.77	289.36	340.21
E_Z (GPa)	86.67	104.73	113.33	173.91
UTS_X (GPa)	30.08	34.20	38.24	44.15
UTS_Z (GPa)	29.12	31.51	34.03	40.23
G_{CX} (GPa)	4.78	5.77	6.16	7.15
G_{CZ} (GPa)	7.19	8.51	9.40	11.22

is considered as ductile, while brittle behavior corresponds to $B_H/G_H \lesssim 1.75$. The brittle and ductile behavior of Li_xCoO_2 based on the Pugh's criterion is shown in Fig. 5. Based on the Pugh's criterion, $LiCoO_2$ is brittle, while CoO_2, $Li_{0.5}CoO_2$, and $Li_{0.75}CoO_2$ are ductile. However, this creterion is based on elastic properties and is too rough to capture all details of large deformations. To characerize the ductility and brittleness of Li_xCoO_2, the simulated tensile tests data are used.

Using the simulated stress-strain curves shown in Figs. 3 and 4, it is clear that $LiCoO_2$ has the highest Young's modulus, or highest stiffness in elastic regions, which is a typical feature of brittle materials. It is also consistent with the predication using the Pugh's criterion. However, when large deformations beyond elastic deformation are considered, using calculated toughness, Gc, as the criterion, single crytal $LiCoO_2$ has the highest ductility among Li_xCoO_2. The order of ductility of Li_xCoO_2 is: $LiCoO_2 > Li_{0.75}CoO_2 > Li_{0.5}CoO_2 > CoO_2$.

As mentioned in the preceding text, Pugh's criterion uses elastic properties to estimate the ductility of the material. The ductility, Gc, can be directly characterized as the area under the stress-strain curve. Larger area means higher ductility. In Figs. 3 and 4, the areas under the stress-strain curves increase with the Li intercalation; this is in contradiction with the Pugh's criterion. Thus Pugh's theory is not an accurate criterion describing Li_xCoO_2.

D. Partial density of states, electron charge transfer, and bond strength

To explain the observed anisotropic lithium content dependent mechanical properties, the PDOS of unstrained Li_xCoO_2 are calculated as shown in Fig. 6. Because the

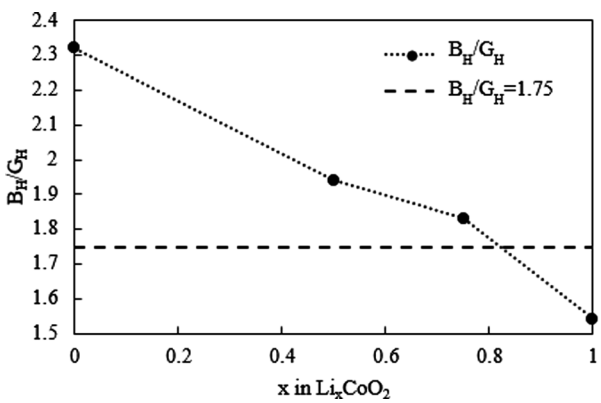

FIG. 5. Pugh's criterion, B_H/G_H, of Li_xCoO_2.

strength of the interatomic bonding and the consequent mechanical response of the materials to deformation are determined primarily by the occupied states just below the Fermi level, the energy range 0–7.5 eV below the Fermi level is used for analysis. It is noted that the contribution of Li to the density of states is very small compared to the Co and O, so the PDOS of Li is not shown here. This result is consistent with both the photoemission spectroscopy and DFT study.[36] It can be seen that in this range, the outermost *d* orbitals of the transition metal Co overlap significantly with the outermost *p* orbitals of the O, indicating a strong *p-d* hybridization. The highest occupied states in Li_xCoO_2 are dominated by Co 3*d* states between −1.5 eV and 0 eV. The PDOS figures show an asymmetry with the Li extraction, which indicates the increasing magnetization. In stoichiometric $LiCoO_2$, Co is not magnetic because the average oxidation state of Co is Co^{3+} with 6 electrons occupying 3*d* orbital. Once Li ions are extracted, the average oxidation state of Co will change, thus making Co become magnetic. This is consistent with the experimental observation.[37] The energy region between −1.5 eV and −8 eV is dominated by O 2*p* states for $LiCoO_2$ and shows a stronger hybridization than Co 3*d* states. With the decrease of x, the energetic overlap of O 2*p* states and the Co 3*d* states increases.

The changes of the *p-d* hybridization orbitals can be characterized by the center of the *d* bands below the Fermi level, as expressed as[38]

$$E_d = \frac{\int_{E_L}^{E_F} PDOS(\mathrm{E,d}) \times EdE}{\int_{E_L}^{E_F} PDOS(\mathrm{E,d})dE}, \quad (1)$$

where E_d is the center of the *d* bands, the Fermi leval E_F is 0, E_L is −7.5 eV to cover the *p-d* hybridization region, PDOS(E,d) is the partial density of states projected onto the d orbitals of the transition metal Co. The calculated E_d for $Li_{0.5}CoO_2$, $Li_{0.75}CoO_2$, and $LiCoO_2$ are −1.98 eV, −2.02 eV, and −2.06 eV, respectively. The stronger the interatomic bond, the lower the E_d value.[38] Hence the center of the *d* bands below the Fermi level provides the insight that $LiCoO_2$ exibits a higher Young's modulus and ulimate strength compared to the delithiated Li_xCoO_2.

To visualize the hybridized electronic states between the transition metal Co and O atoms, the electronic charge distributions are calculated. Figure 7 shows the bonding charge

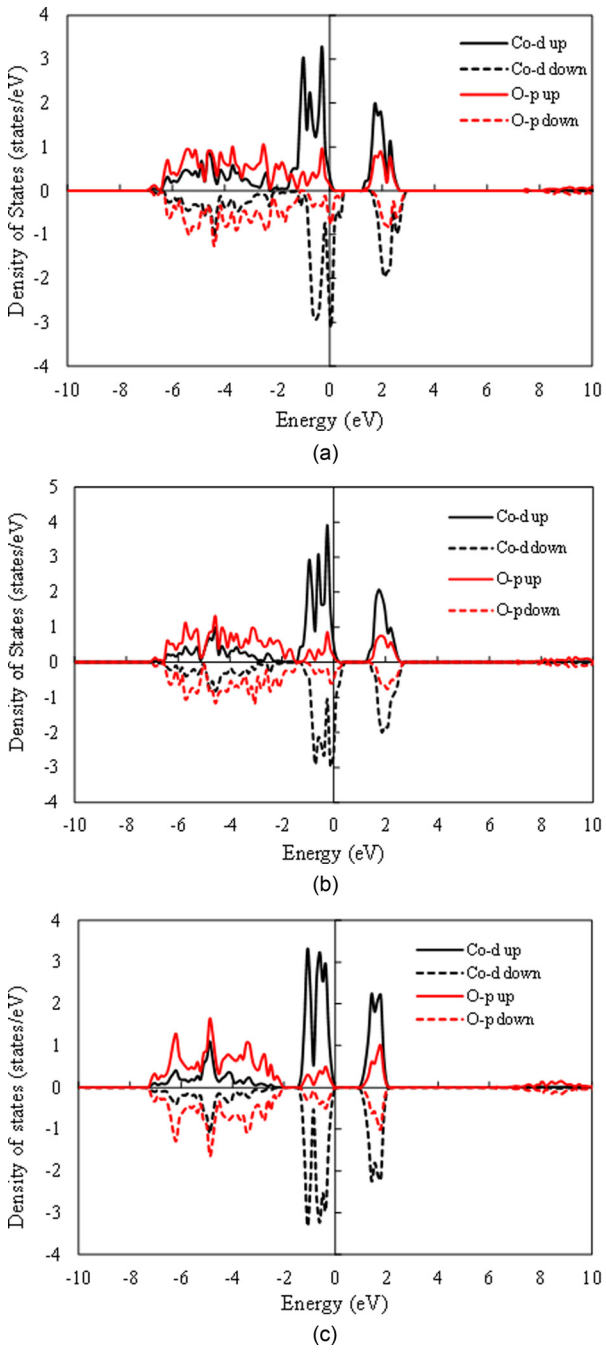

FIG. 6. Partial density of states (PDOS) of Li_xCoO_2 (a) $Li_{0.5}CoO_2$, (b) $Li_{0.75}CoO_2$, (c) $LiCoO_2$.

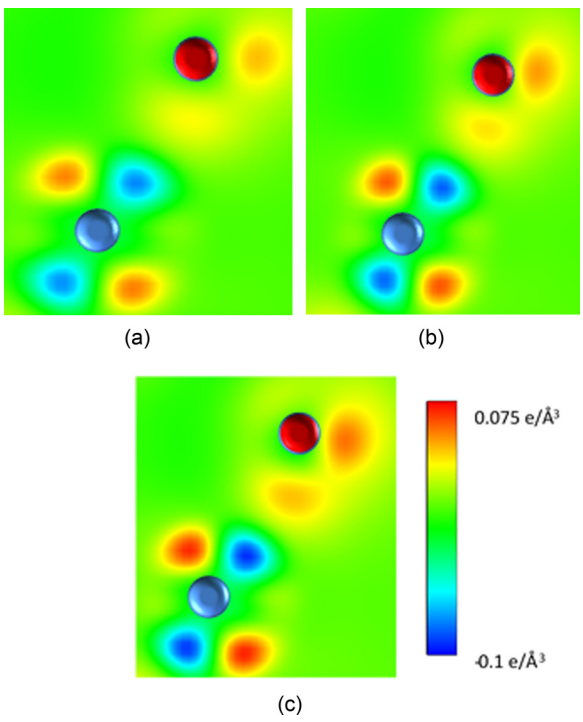

FIG. 7. Charge density difference for Li_xCoO_2. (a) $Li_{0.5}CoO_2$, (b) $Li_{0.75}CoO_2$, (c) $LiCoO_2$. The blue ball is cobalt atom. The red ball is oxygen atom. The view is cut on (44, −21, −1) plane.

density of Li_xCoO_2. The bonding charge density is obtained as the difference between the valence charge density of strain-free Li_xCoO_2 and the superposition of the valence charge density of the constituent atoms. A positive value (red) indicates electron accumulation while a negative value (blue) denotes electron depletion. These bonding charge distributions clearly show the electron accumulation in Li_xCoO_2. The amount of charge localized in this region qualitatively indicates the strength of the Co-O bond. It is obvious that during Li deintercalation, the charge accumulation in the bonding regions become less, indicating a weaker Co-O bond, lower Young's modulus, and ultimate strength.

To further understand the charge transfer quantitively, the magnitude of the charge transfer using Bader charge analysis is conducted.[39] As shown in Fig. 8, the Young's modulus and the ultimate strength along X and Z directions have a linear relationship with both the Li concentration and the charge transfer. It is obvious that the Young's modulus increased with the larger amount of charge transfer. The lithium concentration dependence and anisotropy confirm the previous electron density difference results and also the data in Tables II and IV.

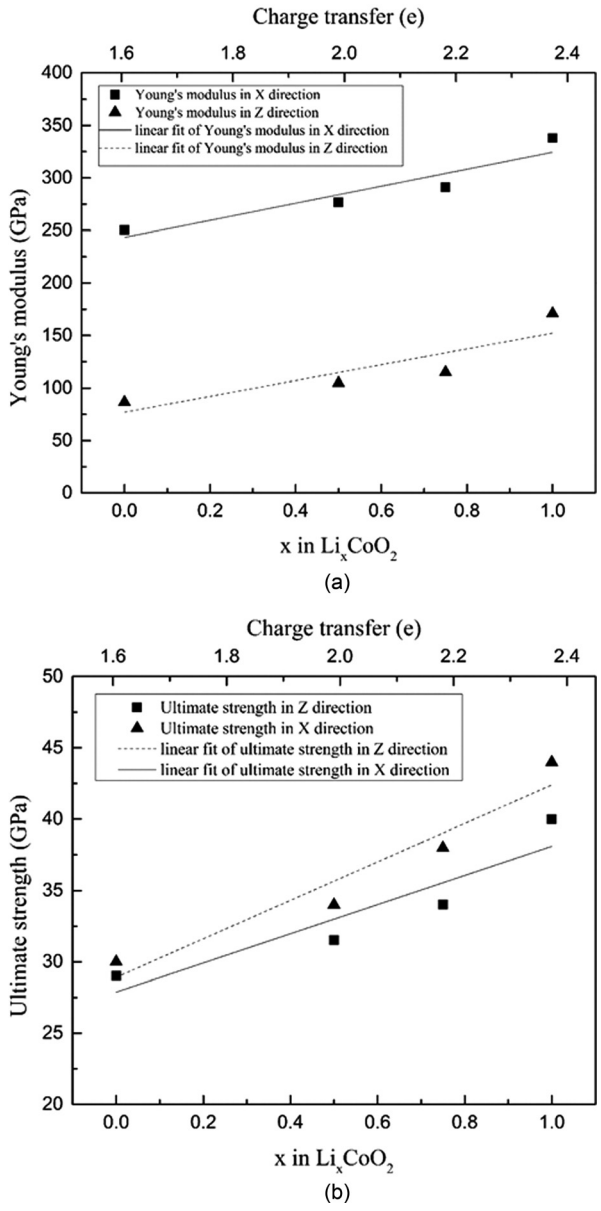

FIG. 8. Young's modulus (a) and ultimate strength (b) as a function of Li concentration and charge transfer of Li_xCoO_2.

TABLE V. Fitted value of $y = m \times \Delta Q + n$ to describe the dependence of Young's modulus Ex and Ey, ultimate strength UTS_X and UTS_Z on charge transfer ΔQ and lithium concentration in Fig. 8.

	m	n
E_X (GPa)	96.74	116.19
E_Z (GPa)	89.68	40.86
UTS_X (GPa)	16.10	7.73
UTS_Z(GPa)	12.21	11.80

The relationship can be conveniently described by a linear relationship $y = m\Delta Q + n$, where ΔQ is the charge transfer, y is the Young's modulus or ultimate strength. The coefficient m and n are listed in Table V. These expressions provide a convenient description of the mechanical properties of Li_xCoO_2, during Li lithiation and delithiation processes.

IV. CONCLUSION

In this paper, the Li content dependent elastic properties have been systematically studied using the first principles calculations. The conclusions are summarized as follows:

(1) The elastic properties under various Li concentrations are computed, and the results are confirmed by simulated *ab initio* tensile tests.
(2) With the increase of the Li concentration ($0.5 < x < 1$), the Young's modulus in X direction increased from 276.77 GPa to 340.21 GPa, meanwhile in Z direction, the Young's modulus increased from 104.73 GPa to 173.91 GPa.
(3) With the increase of the Li concentration ($0.5 < x < 1$), the ultimate strength along X and Z directions increased from 30 GPa to 44 GPa and from 28 GPa to 39 GPa, respectively.
(4) Strong anisotropy of mechanical properties between a-axis and c-axis in Li_xCoO_2 is identified at low lithium concentrations, and the anisotropy decreases with increasing lithium concentration.
(5) Pugh's criterion is not suitable to describe the ductility of Li_xCoO_2.
(6) The observed Li concentration dependent mechanical properties and anisotropy are due to the changes of the Co-O bond strength during Li intercalation. With the increase of Li concentration, the charge accumulation in the bonding regions increases, indicating a strong Co-O bond.
(7) The Young's modulus and ultimate strength of Li_xCoO_2 have a linear relationship with both the Li concentration and the charge transfer. This expression can be used to estimate the Li concentration dependent mechanical properties of Li_xCoO_2.

[1]K. Mizushima, P. C. Jones, P. J. Wiseman, and J. B. Goodenough, "Li_xCoO_2 ($0 < x < 1$): A new cathode material for batteries of high energy density," Mater. Res. Bull. **15**, 783–789 (1980).

[2]B. Huang, Y. I. Jang, Y. M. Chiang, and D. R. Sadoway, "Electrochemical evaluation of $LiCoO_2$ synthesized by decomposition and intercalation of hydroxides for lithium-ion battery applications," J. Appl. Electrochem. **28**, 1365–1369 (1998).
[3]W.-S. Yoon, K.-B. Kim, M.-G. Kim, M.-K. Lee, H.-J. Shin, J.-M. Lee *et al.*, "Oxygen contribution on Li-ion intercalation−deintercalation in $LiCoO_2$ investigated by O K-edge and Co L-edge x-ray absorption spectroscopy," J. Phys. Chem. B **106**, 2526–2532 (2002).
[4]H. Wang, Y. I. Jang, B. Huang, D. R. Sadoway, and Y. M. Chiang, "TEM study of electrochemical cycling-induced damage and disorder in $LiCoO_2$ cathodes for rechargeable lithium batteries," J. Electrochem. Soc. **146**, 473–480 (1999).
[5]F. X. Hart and J. B. Bates, "Lattice model calculation of the strain energy density and other properties of crystalline $LiCoO_2$," J. Appl. Phys. **83**, 7560–7566 (1998).
[6]Y. Qi, L. G. Hector, C. James, and K. J. Kim, "Lithium concentration dependent elastic properties of battery electrode materials from first principles calculations," J. Electrochem. Soc. **161**, F3010–F3018 (2014).
[7]D. R. Diercks, M. Musselman, A. Morgenstern, T. Wilson, M. Kumar, K. Smith *et al.*, "Evidence for anisotropic mechanical behavior and nanoscale chemical heterogeneity in cycled $LiCoO_2$," J. Electrochem. Soc. **161**, F3039–F3045 (2014).
[8]P. Hohenberg and W. Kohn, "Inhomogeneous electron gas," Phys. Rev. **136**, B864–B871 (1964).
[9]W. Kohn and L. J. Sham, "Self-consistent equations including exchange and correlation effects," Phys. Rev. **140**, A1133–A1138 (1965).
[10]J. P. Perdew, K. Burke, and M. Ernzerhof, "Generalized gradient approximation made simple," Phys. Rev. Lett. **77**, 3865–3868 (1996).
[11]J. P. Perdew, K. Burke, and M. Ernzerhof, "Generalized gradient approximation made simple," Phys. Rev. Lett. **78**, 1396–1396 (1997).
[12]P. E. Blöchl, "Projector augmented-wave method," Phys. Rev. B **50**, 17953–17979 (1994).
[13]G. Kresse and D. Joubert, "From ultrasoft pseudopotentials to the projector augmented-wave method," Phys. Rev. B **59**, 1758–1775 (1999).
[14]G. Kresse and J. Furthmüller, "Efficient iterative schemes for *ab initio* total-energy calculations using a plane-wave basis set," Phys. Rev. B **54**, 11169–11186 (1996).
[15]G. Kresse and J. Furthmüller, "Efficiency of ab-initio total energy calculations for metals and semiconductors using a plane-wave basis set," Comput. Mater. Sci. **6**, 15–50 (1996).
[16]S. J. Clark, M. D. Segall, C. J. Pickard, P. J. Hasnip, M. I. J. Probert, K. Refson, and M. C. Payne, "First principles methods using CASTEP," Zeitschrift für Kristallographie – Crystalline Materials **220**, 567–570 (2009).
[17]T. J. Giese and D. M. York, "Density-functional expansion methods: Evaluation of LDA, GGA, and meta-GGA functionals and different integral approximations," J. Chem. Phys. **133**, 244107 (2010).
[18]F. Zhou, M. Cococcioni, C. A. Marianetti, D. Morgan, and G. Ceder, "First-principles prediction of redox potentials in transition-metal compounds with LDA+U," Phys. Rev. B **70**, 235121 (2004).
[19]G. Ceder and A. Van der Ven, "Phase diagrams of lithium transition metal oxides: Investigations from first principles," Electrochim. Acta **45**, 131–150 (1999).
[20]H. J. Monkhorst and J. D. Pack, "Special points for Brillouin-zone integrations," Phys. Rev. B **13**, 5188–5192 (1976).
[21]L. Wu, W. H. Lee, and J. Zhang, "First principles study on the electrochemical, thermal and mechanical properties of $LiCoO_2$ for thin film rechargeable battery," Mater. Today **1**, 82–93 (2014).
[22]T. Motohashi, Y. Katsumata, T. Ono, R. Kanno, M. Karppinen, and H. Yamauchi, "Synthesis and properties of CoO_2, the $x = 0$ end member of the Li_xCoO_2 and Na_xCoO_2 systems," Chem. Mater. **19**, 5063–5066 (2007).
[23]T. Ohzuku, A. Ueda, M. Nagayama, Y. Iwakoshi, and H. Komori, "Comparative study of $LiCoO_2$, $LiNi_{12}Co_{12}O_2$ and $LiNiO_2$ for 4 volt secondary lithium cells," Electrochim. Acta **38**, 1159–1167 (1993).
[24]F. Xiong, H. J. Yan, Y. Chen, B. Xu, J. X. Le, and C. Y. Ouyang, "The atomic and electronic structure changes upon delithiation of $LiCoO_2$: From first principles calculations," Int. J. Electrochem. Sci. **7**, 9390 (2012), available at http://www.electrochemsci.org/papers/vol7/71009390.pdf.
[25]J. N. Reimers and J. R. Dahn, "Electrochemical and in situ x-ray diffraction studies of lithium intercalation in Li_xCoO_2," J. Electrochem. Soc. **139**, 2091–2097 (1992).
[26]A. Van der Ven, M. Aydinol, G. Ceder, G. Kresse, and J. Hafner, "First-principles investigation of phase stability in Li_xCoO_2," Phys. Rev. B **58**, 2975–2987 (1998).
[27]M. Qu, W. H. Woodford, J. M. Maloney, W. C. Carter, Y.-M. Chiang, and K. J. Van Vliet, "Nanomechanical quantification of elastic, plastic, and fracture properties of $LiCoO_2$," Adv. Energy Mater. **2**, 940–944 (2012).
[28]X. Wang, I. Loa, K. Kunc, K. Syassen, and M. Amboage, "Effect of pressure on the structural properties and Raman modes of Li_xCoO_2," Phys. Rev. B **72**, 224102 (2005).
[29]J. M. J. d. Toonder, J. A. W. v. Dommelen, and F. P. T. Baaijens, "The relation between single crystal elasticity and the effective elastic behaviour of polycrystalline materials: Theory, measurement and computation," Modell. Simul. Mater. Sci. Eng. **7**, 909 (1999).
[30]G. G. Amatucci, J. M. Tarascon, and L. C. Klein, "CoO_2, the end member of the Li_xCoO_2 solid solution," J. Electrochem. Soc. **143**, 1114–1123 (1996).
[31]T. A. Manz and D. S. Sholl, "Chemically meaningful atomic charges that reproduce the electrostatic potential in periodic and nonperiodic materials," J. Chem. Theory Comput. **6**, 2455–2468 (2010).
[32]T. A. Manz and D. S. Sholl, "Methods for computing accurate atomic spin moments for collinear and noncollinear magnetism in periodic and nonperiodic materials," J. Chem. Theory Comput. **7**, 4146–4164 (2011).
[33]T. A. Manz and D. S. Sholl, "Improved atoms-in-molecule charge partitioning functional for simultaneously reproducing the electrostatic potential and chemical states in periodic and nonperiodic materials," J. Chem. Theory Comput. **8**, 2844–2867 (2012).
[34]M. A. Caro, S. Schulz, and E. P. O'Reilly, "Comparison of stress and total energy methods for calculation of elastic properties of semiconductors," J. Phys.: Condens. Matter **25**, 025803 (2013).
[35]S. F. Pugh, "XCII. Relations between the elastic moduli and the plastic properties of polycrystalline pure metals," London, Edinburgh, Dublin Philos. Mag. J. Sci. **45**, 823–843 (1954).
[36]D. Ensling, A. Thissen, S. Laubach, P. C. Schmidt, and W. Jaegermann, "Electronic structure of $LiCoO_2$ thin films: A combined photoemission spectroscopy and density functional theory study," Phys. Rev. B **82**, 195431 (2010).
[37]J. T. Hertz, Q. Huang, T. McQueen, T. Klimczuk, J. W. G. Bos, L. Viciu *et al.*, "Magnetism and structure of and comparison to $LiCoO_2$," Phys. Rev. B **77**, 075119 (2008).
[38]J. Li, N. V. Medhekar, and V. B. Shenoy, "Bonding charge density and ultimate strength of monolayer transition metal dichalcogenides," J. Phys. Chem. C **117**, 15842–15848 (2013).
[39]W. Tang, E. Sanville, and G. Henkelman, "A grid-based Bader analysis algorithm without lattice bias," J. Phys.: Condens. Matter **21**, 084204 (2009).
[40]C.-S. Man and M. Huang, "A simple explicit formula for the Voigt-Reuss-Hill average of elastic polycrystals with arbitrary crystal and texture symmetries," J. Elasticity **105**, 29–48 (2011).